Hindawi
International Journal of Polymer Science
Volume 2023, Article ID 6682223, 14 pages
https://doi.org/10.1155/2023/6682223

Research Article

Effects of Gamma Irradiation on the Properties of Hydroxyapatite-Collagen-Chitosan-Mg-ZnO Scaffolds for Bone Tissue Engineering

Tusher -Al-Arafat[1], **Shawon Ahmed**[2], **Polash Chandra Karmakar**[1], **Umme Salma Zohora**[2], **Naznin Akhtar**[1] and **S. M. Asaduzzaman**[1]

[1]*Institute of Tissue Banking and Biomaterial Research, Atomic Energy Research Establishment (AERE), Savar, Dhaka 1349, Bangladesh*
[2]*Department of Biotechnology & Genetic Engineering, Jahangirnagar University, Savar, Dhaka 1342, Bangladesh*

Correspondence should be addressed to S. M. Asaduzzaman; sikderasad@yahoo.com

Received 5 June 2023; Revised 9 October 2023; Accepted 25 October 2023; Published 11 November 2023

Academic Editor: Zhi Li

Bone tissue engineering aims to repair diseased or damaged bone that cannot be regenerated naturally. This study is designed to develop biodegradable porous scaffolds as bone substitutes and evaluate the effect of gamma irradiation on these scaffolds for the restoration of defected bone. Here, composite scaffolds (HA-COL-CS-Mg-ZnO) were prepared by the thermally induced phase separation (TIPS) technique using collagen (COL) and chitosan (CS), hydroxyapatite (HA), magnesium (Mg), and zinc oxide (ZnO) at different mass ratios. Thereafter, the scaffolds were subjected to 10 KGy γ-radiation for physical cross-linking and sterilization. The physicochemical and biological properties of the scaffolds were evaluated by Fourier transform infrared spectroscopy-attenuated total reflectance (FTIR-ATR), field emission scanning electron microscopy (FESEM), physical stability (biodegradability, swelling rate, porosity, and density), mechanical properties, biocompatibility, cytotoxicity, and antimicrobial activity against *Escherichia coli* (ATCC-25922) and *Staphylococcus aureus* (ATCC-25923). We found that the irradiated scaffold showed enhanced tensile strength and antimicrobial activities which are desirable characteristics of bone-mimicking scaffolds. FESEM revealed that the average pore size decreased from 192.3 to 104.5 μm due to radiation. FTIR-ATR spectra showed that γ-radiation triggered cross-linking in the polymer matrix which improved mechanical strength (0.82 N/mm^2 to 1.86 N/mm^2) by increasing pore wall thickness. Moreover, the irradiated and nonirradiated scaffolds were biocompatible and noncytotoxic toward the Vero cell line which ensured their suitability for use *in vivo*. These results demonstrate that sterilization of HA-COL-CS-Mg-ZnO scaffolds with gamma-irradiation substantially improves the physicochemical and morphological features which aid bone tissue regeneration and could be supportive for new bone formation.

1. Introduction

Bone is the basic component of the human skeleton and a widely transplanted organ that provides structure, supports mechanical movement, protects organs, and produces and hosts blood cells [1, 2]. It includes inorganic-organic composite material made up of 50-70% apatite minerals, 20-40% organic (mostly type I collagen), 3% lipids, and 5-10% water [2]. Restoring lost tissue and organs is one of the current challenges in the healthcare sector. Osteoporosis-related bone fractures occur every 20 seconds in people over the age of 50 worldwide [3]. For the treatment of these bone defects, implantable biomaterials such as autografts, allografts, and xenografts are currently being used clinically; however, these approaches have several drawbacks, including postoperative pain, increased blood loss, risk of infectious diseases, scarcity of donors, high costs, immune rejection, and secondary surgical wounds [4]. In order to alleviate these shortcomings, tissue engineering (TE) integrates scaffolds, cells, and physiologically active chemicals to generate functional tissues to

improve tissue regeneration by recapitulating a difference in the physical structure of the tissue [1, 5–7].

Here, scaffolds act as a three-dimensional network that mimics the extracellular matrix, allowing cells to survive, adhere, proliferate, and migrate while maintaining the shape of the regenerated tissue *in vivo*. An ideal biocompatible scaffold has optimal porosity, pore size, a controlled rate of degradation, interconnectivity, suitable mechanical strength, noncytotoxicity, and the ability to initiate chemical signals to direct tissue formation [8, 9].

Although hydroxyapatite (HA) is a natural mineral and cost-effective raw material for the formulation of scaffolds for its biocompatibility, osteoconductivity, osteoinductivity, noninflammatory, and nonimmunogenicity [10, 11], HA has poor mechanical strength that cannot be used as a bulk material for orthopaedic applications [12].

Magnesium (Mg) has favorable mechanical and biological qualities, making it a prospective candidate for human bone repair [13]. In a previous study, a biodegradable Mg/HA composite showed higher compressive strength than HA [14]. Zinc oxide (ZnO) is a promising biodegradable orthopaedic implant material that can be integrated into scaffolds to enhance bone tissue regeneration through antibacterial and mechanical characteristics [15]. By incorporating ZnO into the HA/CS scaffold, the antibacterial properties of ZnO in scaffolds were investigated [16]. In order to elevate the mechanical strength and antimicrobial activity, Mg and ZnO powder can be added with HA which could greatly enhance the range of application for human bone repair.

Collagen (COL), another vital organic component of bone matrix, is a fibrous structural protein found in animals' extracellular matrix and connective tissue and made up of two alpha-1 and one alpha-2 chains [17]. It aids in the repair of broken bones, provides an essential network for cartilage and blood vessel formation, maintains structural integrity, and helps in the cell's biological processes [15, 16, 18]. Besides, chitosan (poly (-(1,4))-2-amino-2-deoxy-d-glucopyranose) (CS) exhibits biocompatibility, bioactivity, biodegradability, antibacterial capabilities, and favorable mechanical properties [16, 17].

Prior to the clinical application of the biomaterials, sterilization is one of the most vital procedures. Gamma radiation is a widely used method for sterilization in the medical industry due to its efficiency, better penetration, effectiveness independent of temperature and pressure conditions, and better certainty of sterility [19]. Gamma irradiation also acts as an essential source for changing scaffolds' internal structure, resulting in many connected alterations in the physicochemical properties of scaffolds making them ideal as bone substitutes [20, 21].

Polymeric scaffolds for biomedical applications have previously been prepared using a variety of approaches, including electrospinning technology, thermally induced phase separation (TIPS) technique, and 3D printing techniques. Among these techniques, TIPS is easy to use, has a low rate of errors, blends well with other manufacturing techniques that can produce scaffolds with high porosity with macro- and micropores up to 90%, and can easily regulate the parameters affecting the scaffold structure like polymer type, solvent, solution concentration, temperature, cooling rate, and additives. This technique also produces three-dimensional network structures that are like naturally occurring extracellular matrix (ECM) [22]. Besides, the bone marrow MSCs cultured on the scaffolds prepared by TIPS exhibited a high degree of osteogenic differentiation, as evidenced by their alkaline phosphatase activity, mineralized matrix formation, and osteocalcin expression *in vitro* [23].

In this study, on the basis of literature on Google Scholar and PubMed from the last 15 years on bone tissue engineering, gamma irradiation, and scaffolds, biomimetic scaffolds were fabricated using HA, COL, CS, ZnO, and Mg through the thermally induced phase separation (TIPS) technique and optimized for their composition. After that, gamma irradiation was applied to these scaffolds as a physical cross-linker as well as a sterilizing agent, and the effect of gamma radiation on their physicochemical properties was analyzed.

2. Materials and Methods

2.1. Extraction of Nanohydroxyapatite (nHA) from Bovine Bone and Collagen from Rabbit Skin. Nanohydroxyapatite (nHA) was derived from bovine bone by the thermal decomposition process [11], and collagen type 1 was extracted from rabbit skin [13] by acetic acid-pepsin treatment. Detailed procedures have been given in the supplementary materials (SM) section.

2.2. Characterization of nHA Powder and Collagen

2.2.1. Fourier Transform Infrared Spectroscopy (FTIR) of nHA and Collagen. The functional groups of the nHA and collagen were detected using FTIR spectroscopy (IRPrestige-21, Japan) in the 400-4000 cm^{-1} range, with a spectral resolution of 4 cm^{-1} and number of scans 12.

2.2.2. X-Ray Powder Diffraction (XRD) of nHA. An X-ray diffractometer (Explorer, GNR Analytical Instruments Group, Italy) was used to analyze the crystalline structure and phase composition of the calcined nHA powder. The scanning angles ranged from 9 to 70 degrees. The working voltage and current were set at 40 kV and 30 mA, respectively, with a 2 s/step counting time [24].

2.2.3. Molecular Weight of Collagen Determination by SDS-PAGE. The molecular weight of collagen was determined using sodium dodecyl sulfate-polyacrylamide gel electrophoresis (SDS-PAGE), and detailed procedures have been given in the SM section.

2.2.4. Nuclear Magnetic Resonance Spectroscopy of Collagen. Collagen (~5 mg) was added to a DMSO solution in an NMR tube and sonicated for 30 minutes. Finally, the sample was analyzed using 5 mm NMR tubes in NMR equipment (Ascend™ 400, Bruker, USA). Liquid-state NMR was conducted at 400.23 MHz with number of scans 16 for ^{1}H and operated at 100.65 and 400.23 MHz with number of scans 1773 for ^{13}C [14].

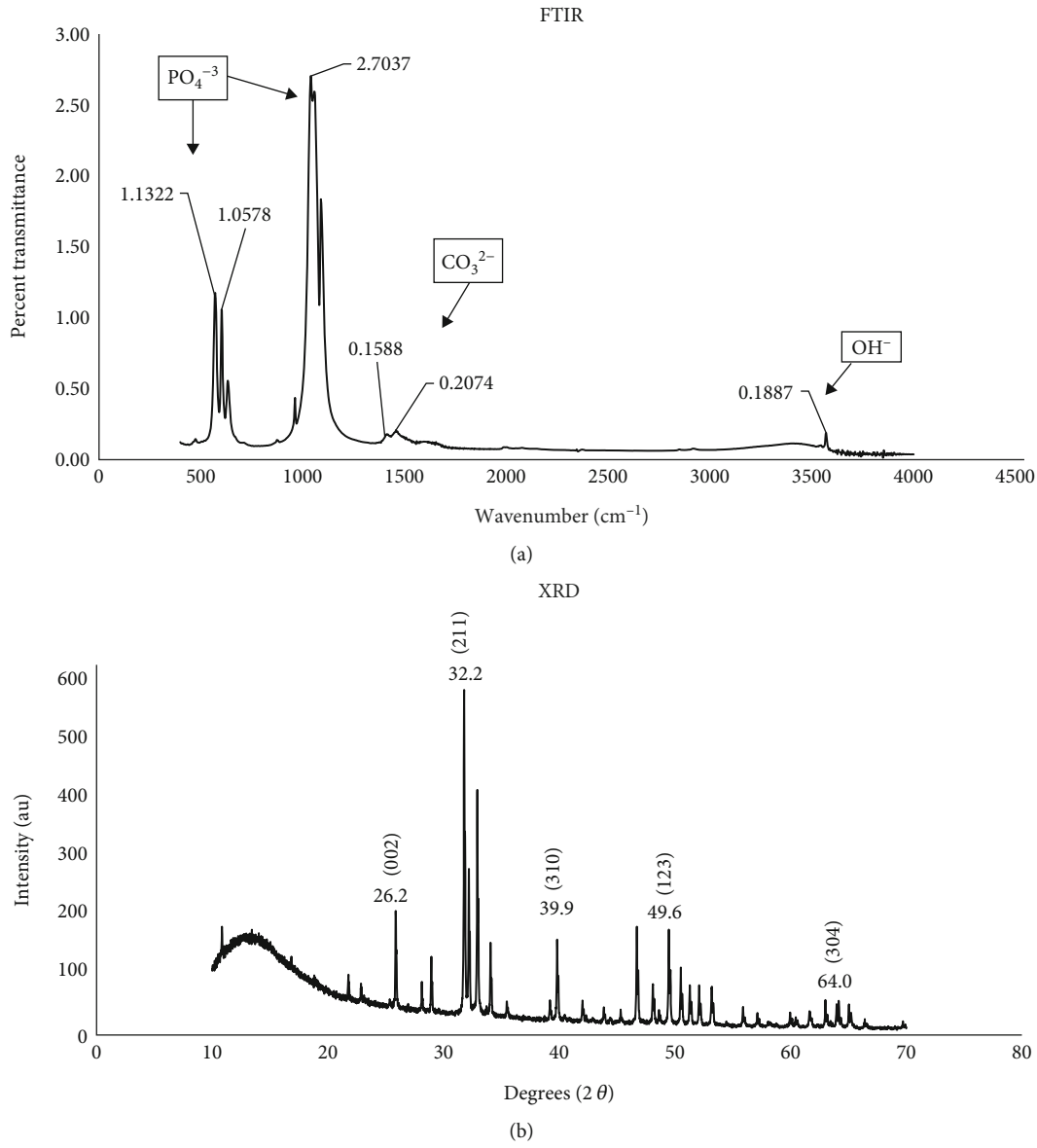

Figure 1: Characterization of nanohydroxyapatite (nHA). (a) Fourier transform infrared spectroscopy (FTIR). (b) Powder X-ray diffraction pattern (XRD) of extracted nHA.

2.3. Fabrication of Scaffolds. Scaffolds were fabricated according to a previously described thermally induced phase separation (TIPS) with some modifications (SM Figure 1), and details of the techniques have been given in the SM section [3].

2.3.1. Fabrication of Hydroxyapatite-Chitosan-Collagen-Mg/ZnO/Mg-ZnO Scaffolds. Scaffolds were fabricated according to a previously described thermally induced phase separation (TIPS) technique with some modifications [4, 25]. Collagen and chitosan powder were weighed as required and dissolved in a 0.5 M acetic acid solution in a 250 ml beaker. The mixture was stirred for 2 hours by stirring at 40°C until the collagen and chitosan powder were thoroughly dispersed in a 0.5 M acetic acid solution. Then, the Mg/ZnO/Mg-ZnO solution was added to the mixture and stirred for 48 hours. The prepared solution was adjusted to about pH 6 using phosphoric acid (H3O4P, Sigma-Aldrich, USA) and stored at 4°C for 24 h.

Finally, nHA powder was weighed as required and dissolved in distilled water. All solutions were mixed and stirred for 5 hours at room temperature to achieve a complete mixture. The resultant solutions were transferred to the petri dish and frozen at -40°C for 48 hours. To obtain scaffolds, the samples were then lyophilized (−80°C, 005 mTorr) for 48 h and stored at the desiccator until further usage. Liquid to solid (L : S) ratio of 94 : 6 was used to fabricate scaffolds with different concentrations of metals (ZnO/Mg/ZnO-Mg), mineral to polymer (M : P) ratio of 2 : 1 with polymer to polymer (P : P) ratios 1 : 1, and gamma irradiation was applied at different doses: 10, 20, and 40 (KGy).

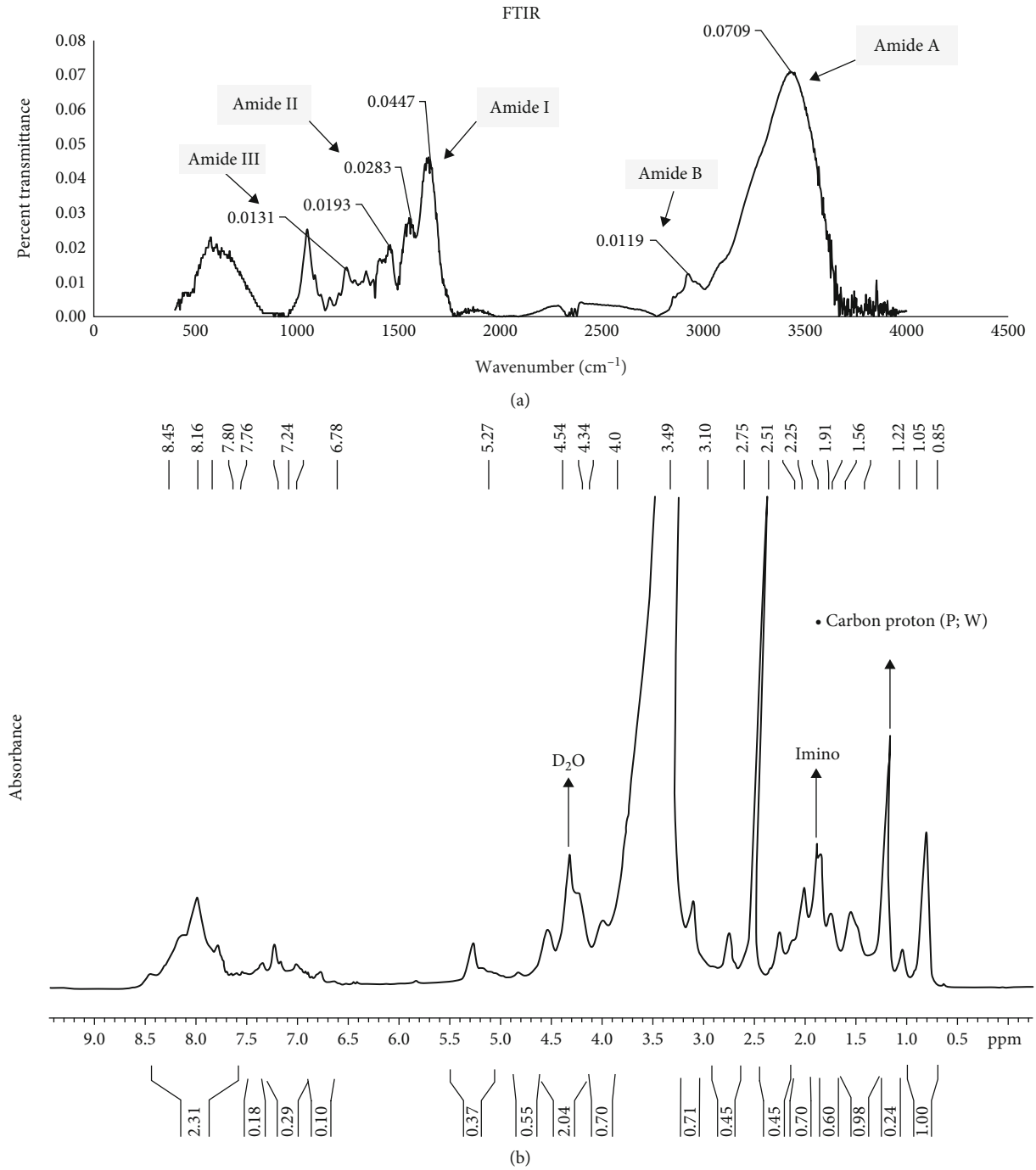

Figure 2: Continued.

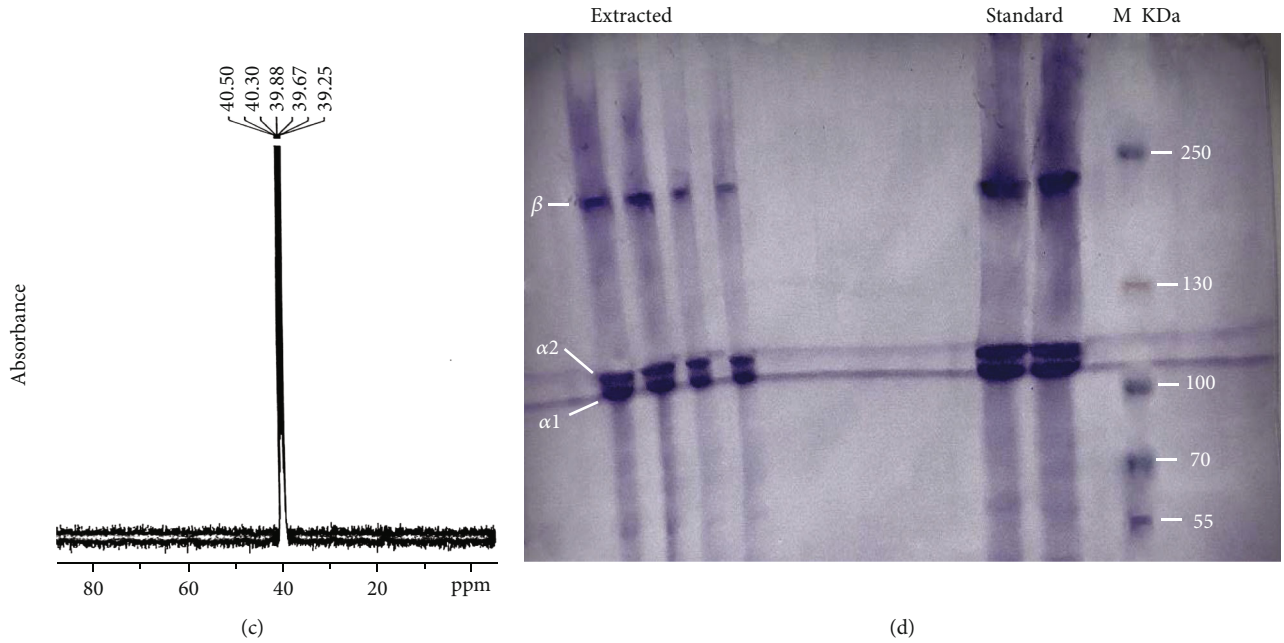

Figure 2: Characterization of collagen. (a) Fourier transform infrared spectroscopy (FTIR) of collagen. (b) Nuclear magnetic resonance (NMR) of collagen (^{1}H). (c) NMR of the collagen (^{13}C). (d) SDS-PAGE of collagen.

2.4. Characterization of Scaffolds. The fabricated scaffolds were characterized by analyzing their porosity, density, swelling ability, and biodegradability, and detailed procedures have been given in the SM section.

2.5. Fourier Transform Infrared Spectroscopy-Attenuated Total Reflectance (FTIR-ATR) Analysis. Fourier transform infrared spectroscopy-attenuated total reflectance (FTIR-ATR) analysis was carried out on the freeze-dried sample using a Nicolet iS5 spectrometer (Thermo Fisher Scientific Inc., USA) with a resolution of 4 cm^{-1} by collecting 32 scans times covering the 400 to 4000 cm^{-1} range, using a diamond ATR accessory model iD7 [26].

2.6. Measurement of Mechanical Properties. The mechanical properties were measured by an electrical universal material testing machine (Shenzhen Wance Testing Machine Co. Ltd., China) with a stretching velocity of 0.5 mm/min. The gauge length, width, and thickness of scaffolds were measured by slide calipers. Force was applied to these sample holders using a lower and upper grip [24]. The tensile strength was calculated from the slope of the stress-strain curve in the linear region, providing the fracture toughness value for samples.

2.7. Blood Biocompatibility Assay. In the blood biocompatibility assay, the scaffold powder was solubilized, and 0.5 ml of the sample was mixed with 1.5 ml of heparinized human blood [4]. Blood samples were mixed at the same ratios with distilled water and isotonic saline water which served as positive and negative controls, respectively. These mixtures were spread on glass slides after 2 hours of incubation at room temperature and observed under a light microscope (Leica ICC50E, Japan).

2.8. Antimicrobial Activity Test. The antibacterial activity of the fabricated scaffolds was performed using the Kirby-Bauer disc diffusion method against two bacterial strains, such as *Escherichia coli* (ATCC-25922) and *Staphylococcus aureus* (ATCC-25923), which are commonly responsible for osteomyelitis and other bone infections [27]. The bacterial colonies were collected and cultured in a nutrient broth medium for 18 hours at 37°C, adjusted to a turbidity of 0.5 McFarland standard (1.00×108 CFU/ml) based on the optical density (OD) measurement at 620 nm [7, 28]. The Mueller-Hinton agar medium (HIMEDIA/M173) was sterilized (121°C for 20 min) for the disc diffusion experiment. Then, two bacteria were cultured for 24 hours on a Mueller-Hinton agar medium. Scaffold samples were allowed to diffuse into the agar plate and incubated at 37°C for 18 hours. The diameter of the growth inhibition zones (mm) surrounding each disc was used to measure antibacterial activity. Doxycycline (commercial antibiotic disc ~30 μg) was used as a positive control, and normal saline (0.9%) was used as a negative control.

2.9. In Vitro Cytotoxicity. The scaffolds were dissolved in nuclease-free water at concentrations of 0.625 mg/ml by a tissue homogenizer. *In vitro* cytotoxicity of scaffolds was measured using the Vero cell line (kidney epithelial cells extracted from an African green monkey) and was maintained in DMEM (Dulbecco's Modified Eagles' medium) containing 1% penicillin-streptomycin (1 : 1), 0.2% gentamycin, and 10% fetal bovine serum (FBS). Cells (3.0×10^{4}/200 μl) were seeded onto a 48-well plate and incubated at 37°C with 5% CO_2. The next day, a 50 μl sample (sterilized) was added to each well. Cytotoxicity was examined under an inverted light microscope after 48 h of incubation. The Vero cell line and the Vero cell

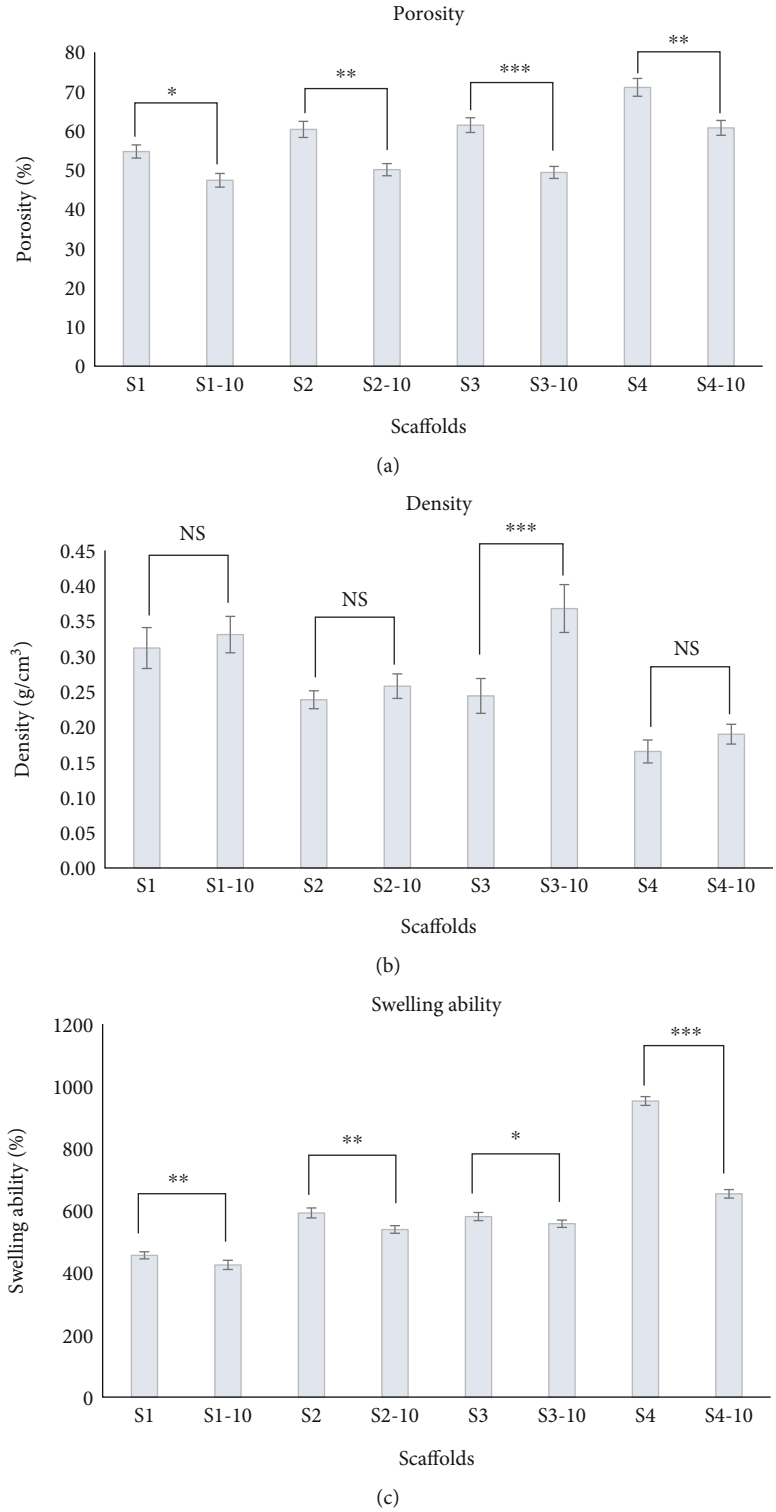

Figure 3: Physicochemical characterization of the HA-COL-CS-Mg/ZnO scaffolds: (a) porosity (%), (b) density (g/cm^3), and (c) swelling ability (%). $^*p \le 0.05$, $^{**}p \le 0.01$, $^{***}p \le 0.001$, and $^{****}p \le 0.0001$.

line with nuclease-free water were considered solvent-negative control and solvent-positive control, respectively. *In vitro* cytotoxicity was also performed by the brine shrimp lethality test, and the procedure of this test has been given in the SM section.

2.10. Field Emission Scanning Electron Microscope (FESEM) Analysis. A field emission scanning electron microscope (FESEM) (JEOL-JSM-7610F, Japan) was used to examine the pore size and surface morphology of the biocomposite scaffolds. Freeze-dried scaffolds were cut into small pieces

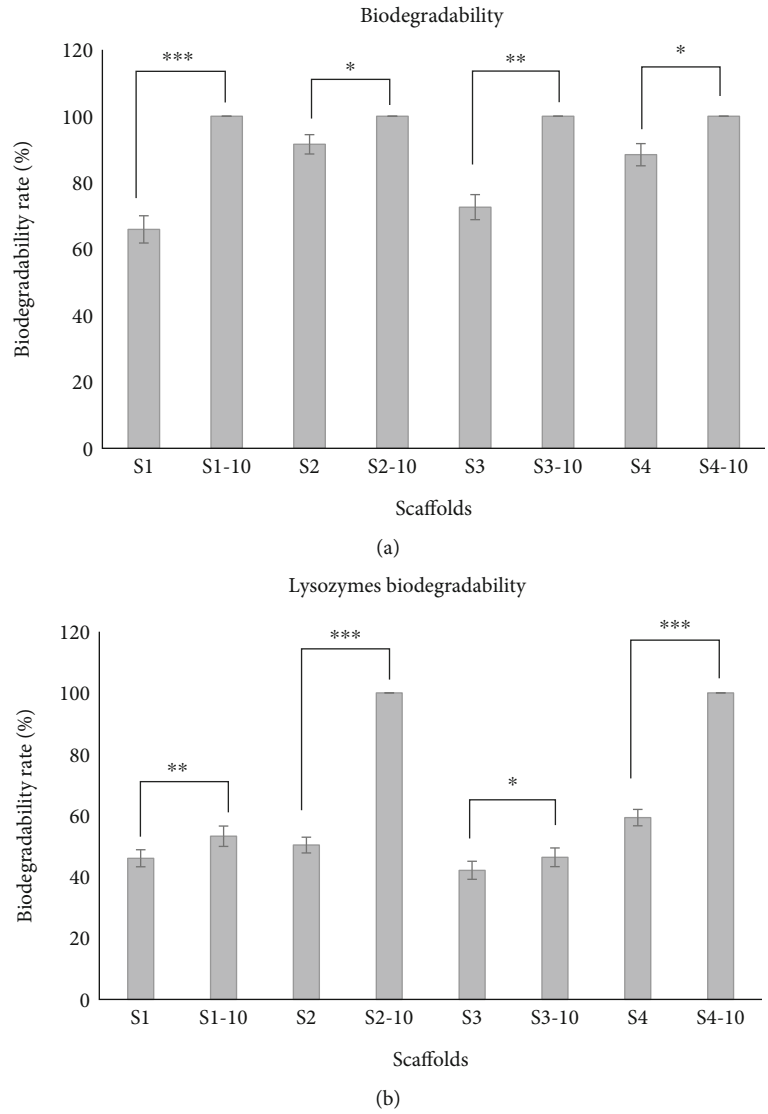

Figure 4: Physicochemical characterization of the HA-COL-CS-Mg/ZnO scaffolds. (a) Biodegradability (%). (b) Lysozymes biodegradability (%). $^{*}p \leq 0.05$, $^{**}p \leq 0.01$, $^{***}p \leq 0.001$, and $^{****}p \leq 0.0001$.

and placed in the autofine coater for 45 s (vacuum pressure at least 2.5 pa) for 1-2 nm platinum coating. After sputtering, samples were mounted on STV which was then placed in the sample holders and finally placed in the FESEM chamber [7].

2.11. Statistical Analysis. Results were expressed as mean ± standard deviation (SD) and SD, as well as p values, were calculated by Student's t-test using Microsoft Excel version 2021. The significant values were considered $^{*}p \leq 0.05$, $^{**}p \leq 0.01$, $^{***}p \leq 0.001$, and $^{****}p \leq 0.0001$.

3. Results and Discussion

3.1. Characterization of Extracted nHA. The final extraction yield of nHA was 47.71%. Details of the extraction yield coefficient have been given in the SM Table 1.

3.2. Fourier Transform Infrared Spectroscopy (FTIR) of nHA. The 570, 601, and 1089 (cm^{-1}) absorbance peaks correspond to the $\upsilon 4$ and $\upsilon 3$ P-O stretching vibration of the phosphate (PO_4^{-3}) group; the existence of carbonate ions (CO_3^{2-}) was confirmed by the peaks at 1411, 1458, and 1597 (cm^{-1}) in the spectra, and similarly, the bands at 3545 and 3570 (cm^{-1}) were linked to the hydroxyl group's (OH^{-}) distinctive stretching modes (Figure 1(a)). The existence of absorbance peaks corresponding to the phosphate, carbonate, and hydroxyl groups in the calcined powder verified the presence of nHA [4]. Similar peaks were observed previously by Rahman et al. and Fernandes et al. [4, 29].

3.3. X-Ray Diffraction of nHA Powder. Diffraction patterns revealed that nHA was present in the calcined powder. The peaks of HA appearing at 26.2°, 32.2°, 49.6°, and 64.0° (2 theta) correspond to the 002, 211, 123, and 304 reflection planes. The XRD pattern of the HA powder obtained is in

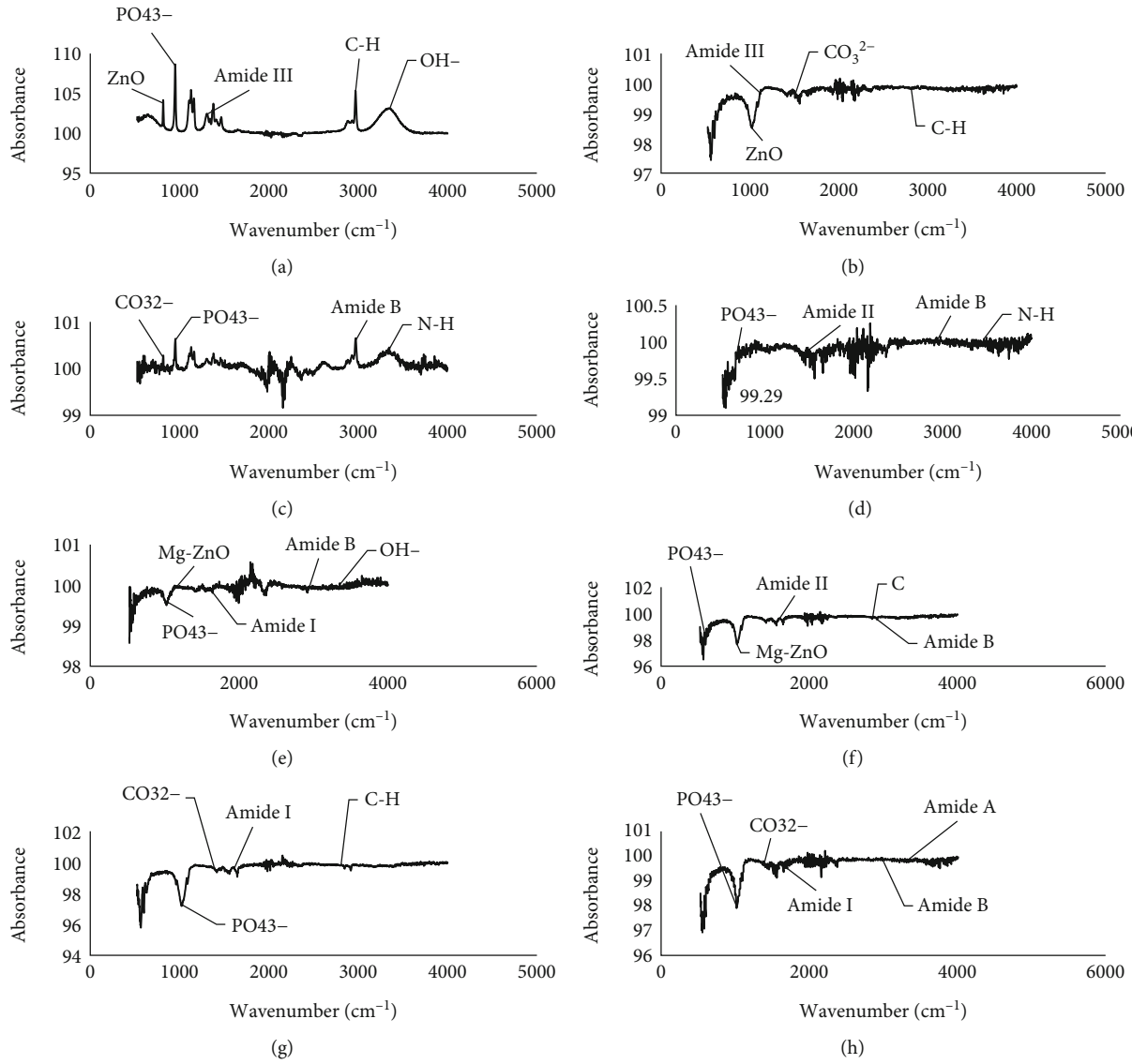

Figure 5: Fourier transform infrared spectroscopy-attenuated total reflectance (FTIR-ATR) spectrum of HA-COL-CS-Mg-ZnO-based scaffolds: (a) S1, (b) S1-10, (c) S2, (d) S2-10, (e) S3, (f) S3-10, (g) S4, and (h) S4-10.

good agreement with the XRD pattern of a HA standard available from the Joint Committee on Powder Diffraction Standards (JCPDS; standard number 84-1998). The peaks at 32.2° (2 theta) position to the 211 plane implied that nHA was highly crystalline, and the intensity of extracted bovine bone-derived nHA was 593.4 au (Figure 1(b)) [30].

3.4. Characterization of Collagen

3.4.1. Fourier Transform Infrared Spectroscopy (FTIR) of Collagen. FTIR confirmed the integrity of the proteins in the conformation of the collagen molecules by detecting all three major amide bands I, II, and III in the regions of 1618-1648, 1534-1545, and 1160-1281 (cm^{-1}), respectively (Figure 2(a)). The C-S stretching vibrations were responsible for the peak in the collagen, which was centered between 570 and 630 cm^{-1}. The protein band at 1400-1450 cm^{-1} was most likely related to C-H bending modes, while the amide A band (NH stretching) and amide B (CH_2 stretching) were found at 3430-3435 cm^{-1} and 2923-3092 cm^{-1}, respectively, which was in accordance with previously performed by Belbachir et al. [31].

3.4.2. Nuclear Magnetic Resonance (NMR) Spectroscopy of Collagen. The ^1H NMR spectra revealed the peaks at 1.228 ppm, 3.109 ppm, and 3.495 ppm were attributed to unfolding amide and α-carbon protons, and the chemical shifts at 1.228 ppm identified proline and tryptophan at extracted collagen (Figure 2(b)). The ^1H NMR spectrum of collagen reported an intense band between 4.002 and 5.279 ppm, presenting the hydration water (D_2O) which stabilized the helical structure by reacting with collagen. The chemical shift of the imino group was observed with a peak at 1.880-1.912 ppm. The ^{13}C NMR spectra also revealed the

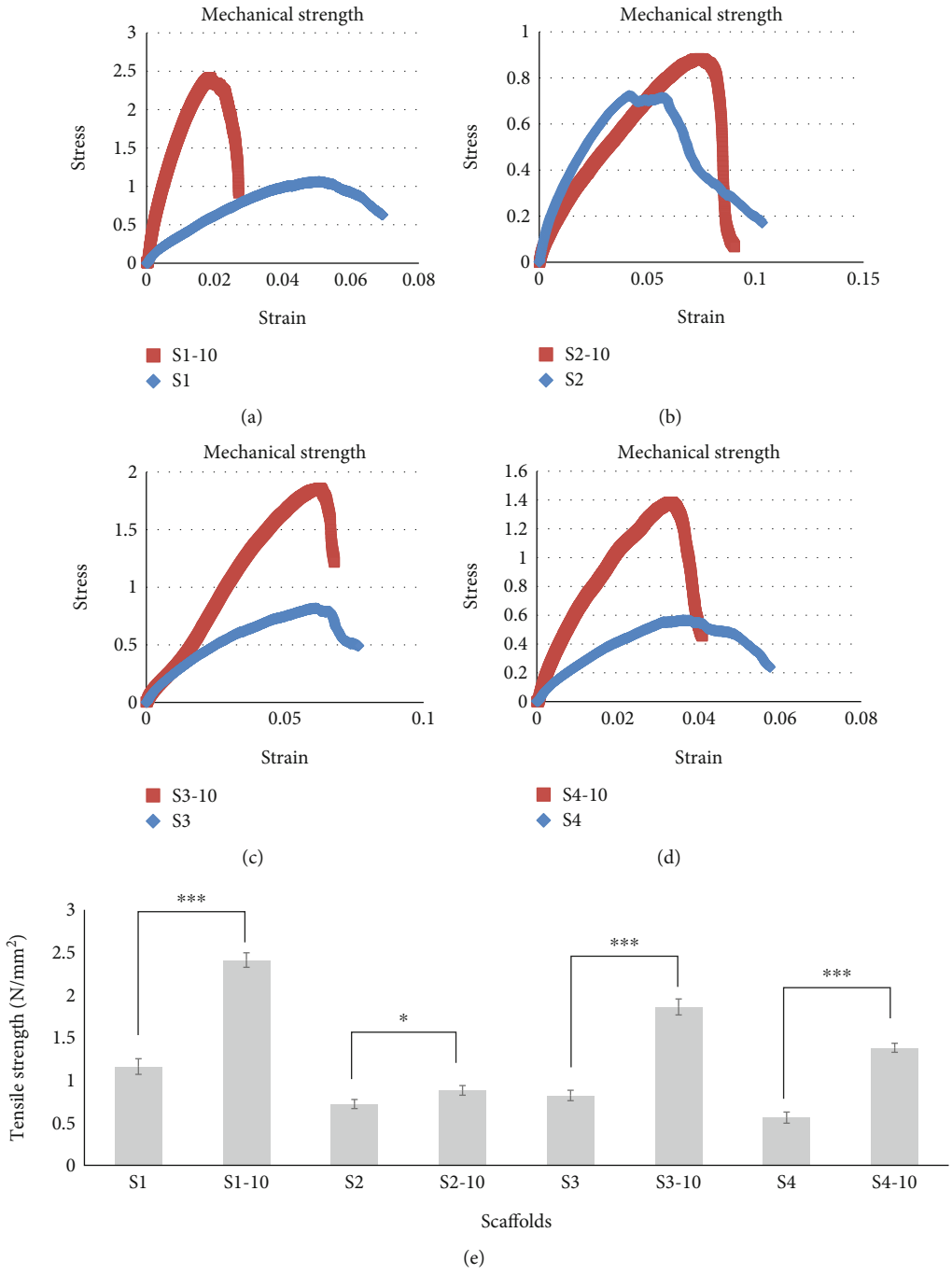

FIGURE 6: Mechanical strength of HA-COL-CS-Mg-ZnO-based scaffolds: (a) S1 and S1-10, (b) S2 and S2-10, (c) S3 and S3-10, (d) S4 and S4-10, and (e) statistical analysis of the mechanical strength of the scaffolds. $^{*}p \leq 0.05$, $^{**}p \leq 0.01$, $^{***}p \leq 0.001$, and $^{****}p \leq 0.0001$.

peaks of the amide bond and some amino acids at 39.25-40.50 ppm (Figure 2(c)) [32].

3.4.3. Molecular Weight Determination of Collagen by SDS-PAGE. The molecular weights of the $\alpha 1$ chain and $\alpha 2$ chain were 102 KDa and 118 KDa, respectively. A third band was produced by cross-linking between two chains called the β chain, and its molecular weight was 220 KDa (Figure 2(d)). This result was similar to the collagen extracted from the rabbit skin conducted by Khodaei et al. [13].

3.4.4. Physicochemical Characterization of the Scaffolds. The ideal porosity for efficiently functionalized scaffolds is 80-90% [33, 34]. The porosity of HA-COL-CS-Mg-ZnO-based scaffolds ranged from 34.41% to 71.03%. The porosity of S1, S2, S3, and S4 was 54.68, 60.33, 61.40, and 71.03, respectively, whereas the values of S1-10, S2-10, S3-10, and S4-10 were 47.36, 50.07, 49.37, and 60.71, respectively. It was observed that porosity was decreasing due to the application of gamma irradiation on these scaffolds (Figure 3(a)).

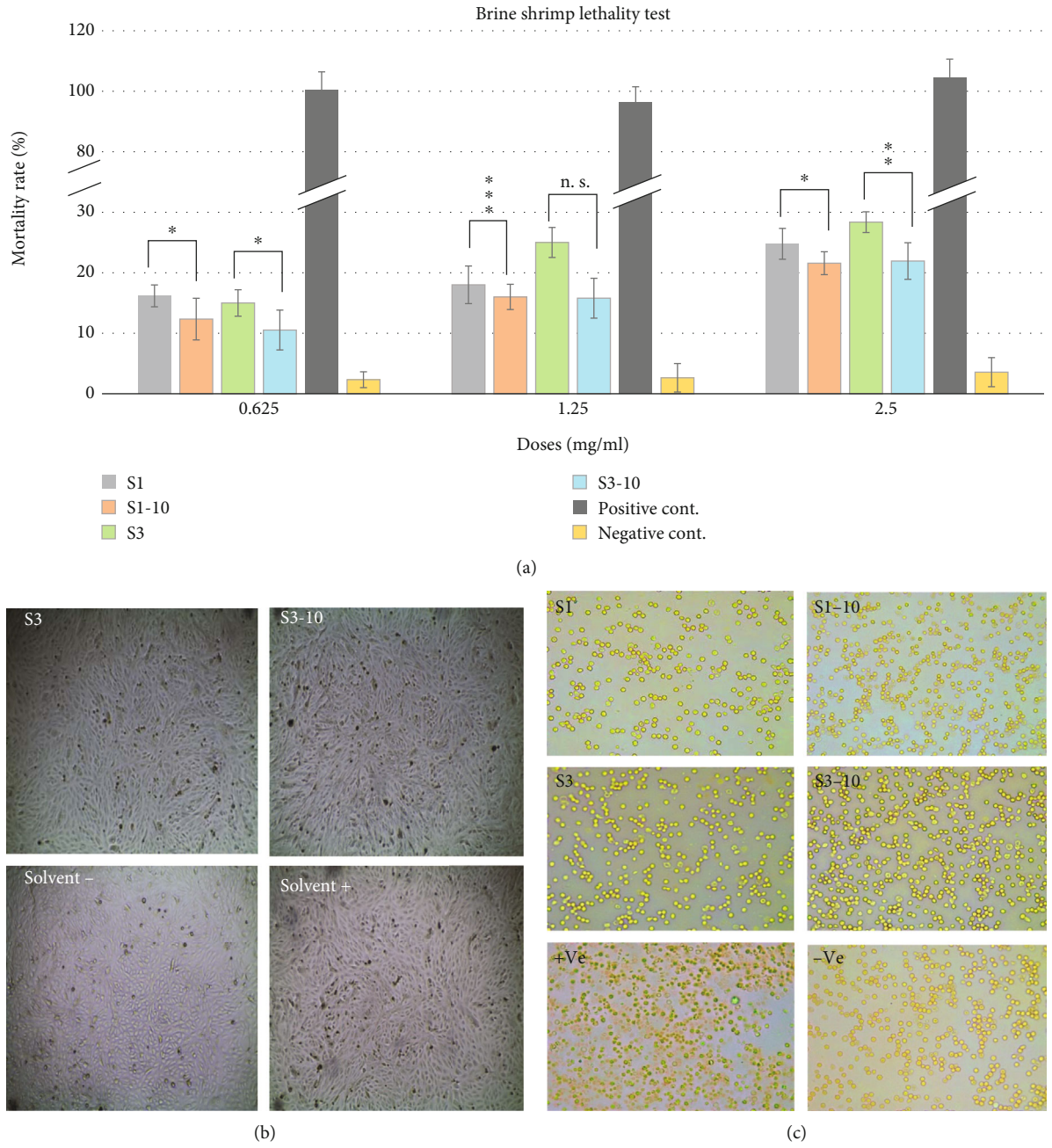

Figure 7: Characterization of HA-COL-CS-Mg-ZnO-based scaffolds. (a) *In vitro* cytotoxicity test by brine shrimp lethality bioassay. (b) Cytotoxicity test of HA-COL-CS-Mg-ZnO scaffolds on Vero cell line. (c) Blood biocompatibility test of HA-COL-CS-Mg-ZnO scaffolds. $^{*}p \le 0.05$, $^{**}p \le 0.01$, $^{***}p \le 0.001$, and $^{****}p \le 0.0001$.

The density of fabricated HA-COL-CS-Mg-ZnO scaffolds ranged from 0.17 g/cm^3 to 0.64 g/cm^3, whereas the apparent density of trabecular bone was reported to range from 1 to 1.4 g/cm^3 [16, 35, 36]. The density of irradiated S3-10 scaffolds was significantly ($p \le 0.001$) higher than that of nonirradiated S3 scaffolds (Figure 3(b)). The swelling rate was significantly decreased after applying radiation (Figure 3(c) and SM Table 2).

The biodegradability of the irradiated S1-10 and S3-10 scaffolds was 75.17% and 80.98% at 21 days (Figure 4(a)), and the biodegradation test using lysozymes reported that S1-10 and S3-10 have a biodegradation rate of 53.25% and 46.37%, respectively (Figure 4(b) and SM Table 3). Scaffolds' biodegradation and density were increased, and porosity and swelling ability were decreased due to applying irradiation.

3.4.5. Fourier Transform Infrared Spectroscopy-Attenuated Total Reflectance (FTIR-ATR) Analysis of HA-COL-CS-Mg-ZnO Scaffolds. The ATR spectra of scaffolds exhibited peaks at 602, 952, and 1035 (cm^{-1}), corresponding to the PO_4^{-3} ion of HA. A small and sharp band was detected at 3572 cm^{-1}

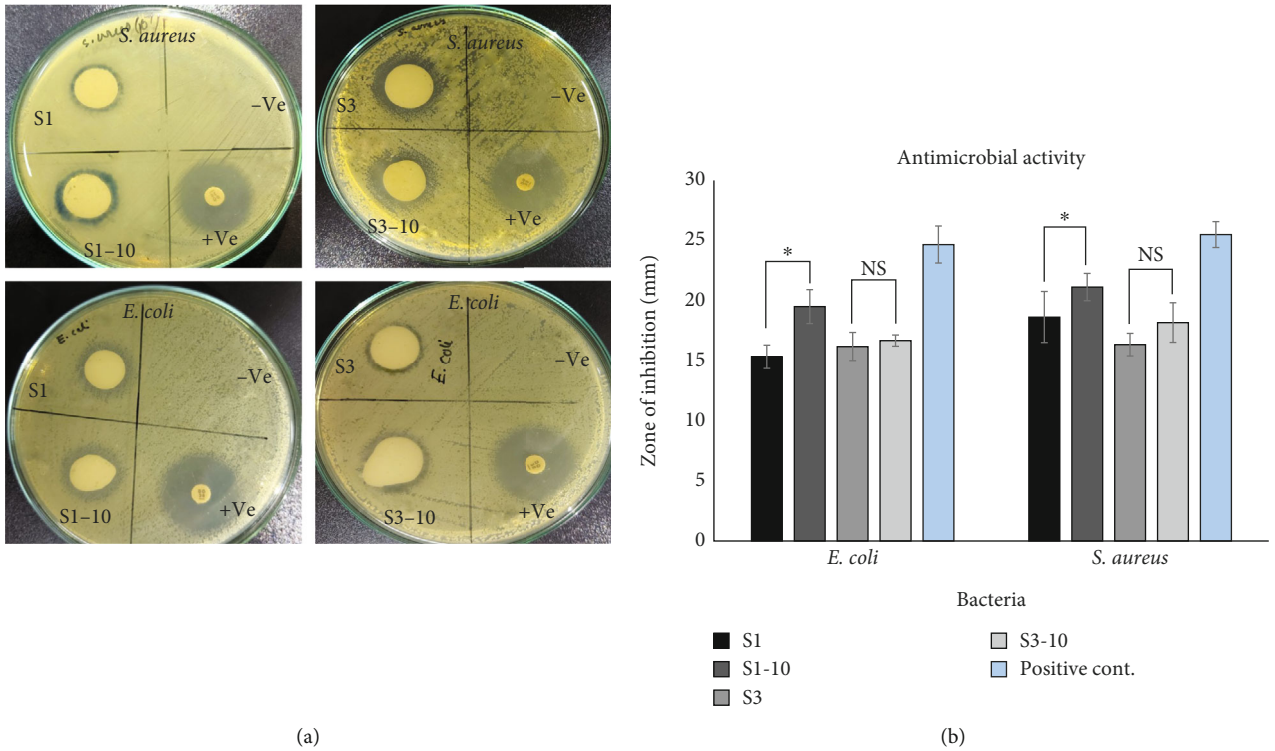

(a) (b)

Figure 8: Characterization of HA-COL-CS-Mg-ZnO-based scaffolds. (a) Antimicrobial activity of the HA-COL-CS-Mg-ZnO scaffolds. (b) Statistical analysis of the zone of inhibition in antimicrobial activity. $^{*}p \leq 0.05$, $^{**}p \leq 0.01$, $^{***}p \leq 0.001$, and $^{****}p \leq 0.0001$.

corresponding to the stretching mode of the OH^- group of HA. A weak peak was observed at 876 cm^{-1}, and a strong peak at 1450 cm^{-1}, which corresponded to the stretching vibration of CO_3^{-2} ions of HA (Figures 5(a)–5(h) and SM Table 4) [29].

The main absorption of HA-COL-CS-Mg-ZnO scaffolds had amide A (3299 cm^{-1}), amide B (2950-2919 cm^{-1}), amide II (1500-1585 cm–1), amide III (1200-1300 cm^{-1}), and amide I (1632-1664 cm^{-1}) with N-H stretching signatures in these composites presented between 3400 and 3440 (cm^{-1}). After applying gamma radiation, amide I was found at 1635-1641 (cm^{-1}), and N-H stretching was at 3213 and 3266 (cm^{-1}) [31]. The spectrum around 3430 cm^{-1} was attributed to the pooled stretching vibration of the OH^- and N-H groups of chitosan. The band at 2845 cm^{-1} corresponded to the C-H bond stretching. The comprehensive bands at 1637 and 1543 (cm^{-1}) were assigned to the existence of the amide I and amide II groups of chitosan. The peak appeared at 562, 843, 1000, and ~4000 (cm^{-1}) due to Mg metal and ZnO incorporated in these scaffolds.

The functional groups of HA-COL-CS-Mg-ZnO-based scaffolds in the ATR spectrum were similar to the study of Rahman et al. [4], but some differences in the spectrum range (Figures 5(a)–5(h)) were due to the different polymer, mineral ratios, and incorporation of metallic materials (Mg/ZnO/Mg-ZnO) with a 10 KGy irradiation dose.

3.4.6. Mechanical Test of HA-COL-CS-Mg-ZnO-Based Scaffolds. The mechanical strength of nonirradiated scaffolds S1, S2, S3, and S4 were 1.06, 0.72, 0.82, and 0.56, and the irradiated scaffolds were 2.41, 0.88, 1.86, and 1.38, respectively (Figures 6(a)–6(d) and SM Table 5). The mechanical strength increased significantly due to radiation (Figure 6(e)). Qu et al. reported that the tensile strength of bones (vertebra, tibia, and femur) ranges from 2.4 to 6.8 N/mm^2, whereas the tensile strength of S3 and S3-10 was 0.82 N/mm^2 and 1.86 N/mm^2, respectively [37].

3.4.7. In Vitro Cytotoxicity Test of HA-COL-CS-Mg-ZnO-Based Scaffolds. The mortality rate of nonirradiated scaffolds S1 and S3 was 16.18 ± 1.80 and 15 ± 2.18, whereas for irradiated scaffolds S1-10 and S3-10, it was 12.33 ± 3.44 and 10.53 ± 3.30, respectively, at a concentration of 0.625 mg/ml. The brine shrimp lethality test suggested that the mortality rate decreased with 10 KGy irradiation doses on scaffolds (Figure 7(a)).

The survivability rate of Vero cells in S3 and S3-10 scaffolds was more than 95% at 0.625 mg/ml. There was no difference between irradiated (S3-10) and nonirradiated (S3) scaffolds. The Vero cell line was used as a solvent negative that showed 100% survival of Vero cells in the culture plate. Both the irradiated and nonirradiated scaffolds were noncytotoxic in the Vero cell line (Figure 7(b)).

The biocompatibility and functionality of the scaffolds can be greatly enhanced by coating them with biomolecules via antigen/antibody, DNA hybridization, or ligand/receptor interactions to provide biological and mechanical support for bone abnormalities [38]. In our future study, we will incorporate biomolecules via antigen/antibody and DNA hybridization with scaffolds to enhance biocompatibility and functionality.

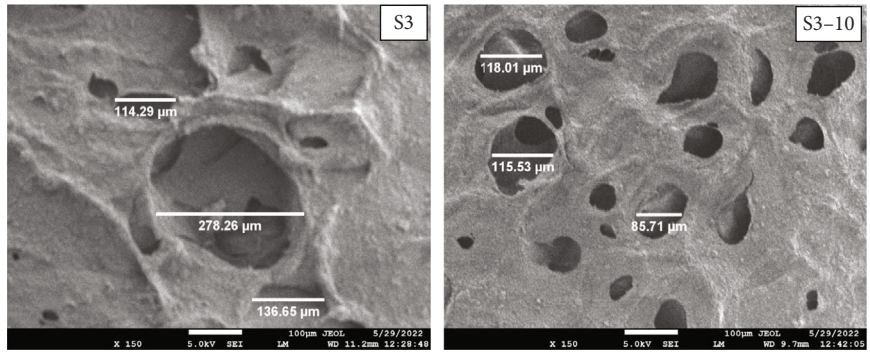

Figure 9: Field emission scanning electron microscopy (FESEM) of HA-COL-CS-Mg-ZnO-based scaffolds.

3.4.8. Blood Biocompatibility of HA-COL-CS-Mg-ZnO-Based Scaffolds. Cell damage occurred in the positive control due to the osmotic shock, and the negative control showed an intact morphology of RBC. Resistance of the blood cells toward deformation in the presence of HA-COL-CS-Mg-ZnO-based scaffolds is shown in Figure 7(c), where gamma-irradiated scaffolds S1-10 and S3-10 were more biocompatible than nonirradiated S1 and S3 scaffolds.

3.4.9. Antimicrobial Activity of HA-COL-CS-mg-ZnO Based Scaffold. The zone of inhibition for the irradiated samples S1-10 and S3-10 was greater than for the nonirradiated samples S1 and S3 against both *Staphylococcus aureus* and *Escherichia coli* (Figures 8(a) and 8(b)) which are also responsible for bone infection [39, 40].

3.4.10. Field Emission Scanning Electron Microscope (FESEM) Analysis of Scaffolds. The average pore size of the nonirradiated S3 (HA-COL-CS-Mg-ZnO) and irradiated (S3-10) scaffolds was 207.24 μm and 120.25 μm, respectively, which is demonstrated in Figure 9 and SM Figure 2. Here, the pore diameter was decreased after applying gamma irradiation on these scaffolds.

For effectively functionalized scaffolds, the optimal pore diameter is 200-400 μm; therefore, the pore diameter of the fabricated S3 scaffold was favorable for osteoblast proliferation and migration for bone tissue engineering [33, 41].

4. Conclusion

Our study demonstrated that the irradiated HA-COL-CS-Mg-ZnO scaffold exhibited desirable physicochemical properties including enhanced tensile strength and antimicrobial activities, a functionalized ATR spectrum, and noncytotoxic toward the Vero cell line which would meet the basic requirements for bone tissue engineering. Since the manufactured scaffold has all the criteria of becoming an ideal scaffold, in the future, the scaffolds incorporated with green nanomaterials (environmentally friendly, which effectively avoid disadvantages of conventional physical and chemical technologies, such as toxicity, pollution, and uneconomical and complicated operation) as well as stem cells and growth factors targeting bone cells will be applied preclinically against various osteogenic metabolic disorders.

Data Availability

The datasets used and/or analyzed during the current study are available from the corresponding author upon reasonable request.

Ethical Approval

The "Ethical Review Committee" of Jahangirnagar University, Savar, Dhaka, Bangladesh, has provided ethical permission (Ref No: BBEC, JU/M 2022/7(2)) for the extraction of collagen from rabbits' skin.

Conflicts of Interest

The authors declare no conflict of interest.

Authors' Contributions

Tusher -Al-Arafat provided substantial contributions to the conceptualization, data curation, formal analysis, investigation, supervision, validation, writing—original draft, and writing—review and editing. Shawon Ahmed was involved in the conceptualization, data curation, formal analysis, investigation, validation, and writing—original draft. Polash Chandra Karmakar helped with the conceptualization, data curation, formal analysis, investigation, validation, writing—original draft, and writing—review and editing. Umme Salma Zohora contributed to the formal analysis, investigation, validation, and writing—original draft. Naznin Akhtar was assigned to investigation, validation, and writing—review and editing. S. M. Asaduzzaman worked on conceptualization, data curation, formal analysis, investigation, supervision, validation, writing—original draft, and writing—review and editing. Tusher -Al-Arafat, Shawon Ahmed, and Polash Chandra Karmakar contributed equally to this work.

Acknowledgments

This experimental study was supported by the Research and Development Project from the Ministry of Science and Technology, Bangladesh.

Supplementary Materials

The detailed procedures of extraction of nHA from bovine bone, fabrication of scaffolds, extraction and SDS-PAGE of collagen, physiochemical characterization of scaffolds (porosity and density, swelling ratio, and in vitro biodegradability), in vitro blood biocompatibility assay, brine shrimp lethality test, and antibacterial activity test have been mentioned in the supplementary materials (SM) section. SM Figure 1: hydroxyapatite-chitosan-collagen (HA-COL-CS)-Mg-ZnO-based scaffolds, S1 [HA-COL-CS-ZnO], S2 [HA-COL-CS-Mg], S3 [HA-COL-CS-ZnO-Mg], S4 [HA-COL-CS]. SM Table 1: extraction yield coefficient of nHA. SM Table 2: physiochemical study of HA-COL-CS-ZnO-Mg scaffolds. SM Table 3: biodegradability study of HA-COL-CS-Mg-ZnO scaffolds. SM Table 4: functional groups of HA-COL-CS-Mg-ZnO scaffolds in the ATR spectrum. SM Table 5: mechanical strength of HA-COL-CS-Mg-ZnO scaffolds. *(Supplementary Materials)*

References

[1] M. N. Collins, G. Ren, K. Young, S. Pina, R. L. Reis, and J. M. Oliveira, "Scaffold fabrication technologies and structure/function properties in bone tissue engineering," *Advanced Functional Materials*, vol. 31, no. 21, 2021.

[2] Y. P. Guo, J. J. Guan, J. Yang, Y. Wang, C. Q. Zhang, and Q. F. Ke, "Hybrid nanostructured hydroxyapatite-chitosan composite scaffold: bioinspired fabrication, mechanical properties and biological properties," *Journal of Materials Chemistry B*, vol. 3, no. 23, pp. 4679–4689, 2015.

[3] N. Abbasi, S. Hamlet, R. M. Love, and N. T. Nguyen, "Porous scaffolds for bone regeneration," *Journal of Science: Advanced Materials and Devices*, vol. 5, no. 1, pp. 1–9, 2020.

[4] M. S. Rahman, M. M. Rana, L. S. Spitzhorn et al., "Fabrication of biocompatible porous scaffolds based on hydroxyapatite/collagen/chitosan composite for restoration of defected maxillofacial mandible bone," *Progress in Biomaterials*, vol. 8, no. 3, pp. 137–154, 2019.

[5] E. Ahmadian, A. Eftekhari, D. Janas, and P. Vahedi, "Nanofiber scaffolds based on extracellular matrix for articular cartilage engineering: a perspective," *Nano*, vol. 7, no. 1, pp. 61–69, 2023.

[6] E. Barua, P. Deb, S. Das Lala, and A. B. Deoghare, "Extraction of hydroxyapatite from bovine bone for sustainable development," in *Biomaterials in Orthopaedics and Bone Regeneration*, Springer, Singapore, 2019.

[7] T. Sultana, M. Rana, M. Akhtar, Z. Hasan, A. H. Talukder, and S. M. Aseduzzaman, "Preparation and physicochemical characterization of nano-hydroxyapatite-based 3D porous scaffold for biomedical application," *Advances in Tissue Engineering and Regenerative Medicine*, vol. 3, no. 3, article 00065, 2017.

[8] B. T. Edwin, H. Dhanya, P. D. Nair, and M. Kassem, "In vitro and in vivo evaluation of 1-(3 dimethylaminopropyl)-3-ethyl carbodiimide (EDC) cross-linked gum Arabic–gelatin composite as an ideal porous scaffold for tissue engineering," in *Biomaterials in Orthopaedics and Bone Regeneration*, Springer, Singapore, 2019.

[9] G. Singh, A. S. Bhui, S. S. Sidhu, P. S. Bains, and Y. Lamichhane, "Surface characteristics and in vitro corrosion behavior of HAp-coated 316L stainless steel for biomedical applications," in *Biomaterials in Orthopaedics and Bone Regeneration*, Springer, Singapore, 2019.

[10] J. Huang, J. Ratnayake, N. Ramesh, and G. J. Dias, "Development and characterization of a biocomposite material from chitosan and New Zealand-sourced bovine-derived hydroxyapatite for bone regeneration," *ACS Omega*, vol. 5, no. 27, pp. 16537–16546, 2020.

[11] M. A. Martínez-Ortiz, A. D. Hernández-Fuentes, D. J. Pimentel-González, R. G. Campos-Montiel, A. Vargas-Torres, and G. Aguirre-Álvarez, "Extraction and characterization of collagen from rabbit skin: partial characterization," *CyTA-Journal of Food*, vol. 13, no. 2, pp. 253–258, 2015.

[12] I. Ielo, G. Calabrese, G. De Luca, and S. Conoci, "Recent advances in hydroxyapatite-based biocomposites for bone tissue regeneration in orthopedics," *International Journal of Molecular Sciences*, vol. 23, no. 17, p. 9721, 2022.

[13] M. Khodaei, F. Nejatidanesh, M. J. Shirani, S. Iyengar, H. Sina, and O. Savabi, "Magnesium/Nano-hydroxyapatite composite for bone reconstruction: the effect of processing method," *Journal of Bionic Engineering*, vol. 17, no. 1, pp. 92–99, 2020.

[14] M. M. F. Aizat, M. R. N. Liyana, and K. S. Khalijah, "Fabrication of magnesium-hydroxyapatite composites targeted for biodegradable implant application," *AIP Conference Proceedings*, vol. 2030, no. 1, 2018.

[15] D. Zhang, N. Ni, Y. Su et al., "Targeting local osteogenic and ancillary cells by mechanobiologically optimized magnesium scaffolds for orbital bone reconstruction in canines," *ACS applied Materials & Interfaces*, vol. 12, no. 25, pp. 27889–27904, 2020.

[16] A. H. Yuwono, G. Ramahdita, M. A. Mu'lanuddin, A. Adyandra, and G. Gustiraharjo, "The study of zinc oxide addition into hydroxyapatite/chitosan scaffold for bone tissue engineering application," *AIP Conference Proceedings*, vol. 2193, no. 1, 2019.

[17] V. Saxena, A. Hasan, and L. M. Pandey, "Antibacterial nanobiocomposite scaffolds of chitosan, carboxymethyl cellulose and Zn & Fe integrated hydroxyapatite (chitosan-CMC-FZO@HAp) for bone tissue engineering," *Cellulose*, vol. 28, no. 14, pp. 9207–9226, 2021.

[18] S. Prasadh, V. Ratheesh, V. Manakari, G. Parande, M. Gupta, and R. Wong, "The potential of magnesium based materials in mandibular reconstruction," *Metals (Basel)*, vol. 9, no. 3, p. 302, 2019.

[19] C. R. Harrell, V. Djonov, C. Fellabaum, and V. Volarevic, "Risks of using sterilization by gamma radiation: the other side of the coin," *International Journal of Medical Sciences*, vol. 15, no. 3, pp. 274–279, 2018.

[20] J. X. Jiang, L. M. Li, L. L. Lin, Y. Zuo, Y. B. Li, and J. D. Li, "Effects of γ-ray irradiation on the properties of nano-hydroxyapatite/polyurethane composite porous scaffolds," *Materials Science Forum*, vol. 852, pp. 422–427, 2016.

[21] F. You, Y. Li, Y. Zuo, and J. Li, "The influence of γ-ray irradiation on the mechanical and thermal behaviors of nHA/PA66 composite scaffolds," *Scientific World Journal*, vol. 2013, pp. 1–6, 2013.

[22] A. Cahyanto, K. Tsuru, K. Ishikawa, and M. Kikuchi, "Mechanical strength improvement of apatite cement using hydroxyapatite/collagen nanocomposite," in *Key Engineering Materials*, pp. 167–172, Trans Tech Publications Ltd, 2016.

[23] T. Zhang, K. Chen, X. Wu, and X. Xiao, "Preparation of nanofibrous poly (L-lactic acid) scaffolds using the thermally

induced phase separation technique in dioxane/polyethylene glycol solution," *Designed Monomers and Polymers*, vol. 26, no. 1, pp. 77–89, 2023.

[24] L. Roseti, V. Parisi, M. Petretta et al., "Scaffolds for bone tissue engineering: state of the art and new perspectives," *Materials Science and Engineering: C*, vol. 78, no. 1246-1262, pp. 1246–1262, 2017.

[25] S. I. Kim, N. E. Kim, S. Park et al., "Characterization of non-solvent-and thermal-induced phase separation applied polycaprolactone/demineralized bone matrix scaffold for bone tissue engineering," *In Vitro models*, vol. 1, no. 2, pp. 197–207, 2022.

[26] M. Mulazzi, E. Campodoni, G. Bassi et al., "Medicated hydroxyapatite/collagen hybrid scaffolds for bone regeneration and local antimicrobial therapy to prevent bone infections," *Pharmaceutics*, vol. 13, no. 7, p. 1090, 2021.

[27] M. Lu, J. Liao, J. Dong et al., "An effective treatment of experimental osteomyelitis using the antimicrobial titanium/silver-containing nHP66 (nano-hydroxyapatite/polyamide-66) nanoscaffold biomaterials," *Scientific Reports*, vol. 6, no. 1, 2016.

[28] C. Li, W. Qin, S. Lakshmanan, X. Ma, X. Sun, and B. Xu, "Hydroxyapatite based biocomposite scaffold: a highly biocompatible material for bone regeneration," *Saudi Journal of Biological Sciences*, vol. 27, no. 8, pp. 2143–2148, 2020.

[29] L. L. Fernandes, C. X. Resende, D. S. Tavares, G. A. Soares, L. O. Castro, and J. M. Granjeiro, "Cytocompatibility of chitosan and collagen-chitosan scaffolds for tissue engineering," *Polímeros*, vol. 21, pp. 1–6, 2011.

[30] A. Chandrasekar, S. Sagadevan, and A. Dakshnamoorthy, "Synthesis and characterization of nano-hydroxyapatite (n-HAP) using the wet chemical technique," *International Journal of Physical Science*, vol. 8, no. 32, pp. 1639–1645, 2013.

[31] K. Belbachir, R. Noreen, G. Gouspillou, and C. Petibois, "Collagen types analysis and differentiation by FTIR spectroscopy," *Analytical and Bioanalytical Chemistry*, vol. 395, no. 3, pp. 829–837, 2009.

[32] R. Consonni, L. Santomo, R. Tenni, R. Longhi, and L. Zetta, "Conformational study of a collagen peptide by 1H NMR spectroscopy: observation of the 14N-1H spin-spin coupling of the Arg guanidinium moiety in the triple-helix structure," *FEBS Letters*, vol. 436, no. 2, pp. 243–246, 1998.

[33] K. Akeda, H. S. An, M. Okuma et al., "Platelet-rich plasma stimulates porcine articular chondrocyte proliferation and matrix biosynthesis," *Osteoarthritis and Cartilage*, vol. 14, no. 12, pp. 1272–1280, 2006.

[34] N. Zhang, H. L. Nichols, S. Tylor, and X. Wen, "Fabrication of nanocrystalline hydroxyapatite doped degradable composite hollow fiber for guided and biomimetic bone tissue engineering," *Materials Science and Engineering: C*, vol. 27, no. 3, pp. 599–606, 2007.

[35] L. Malladi, A. Mahapatro, and A. S. Gomes, "Fabrication of magnesium-based metallic scaffolds for bone tissue engineering," *Materials and Technologies*, vol. 33, no. 2, pp. 173–182, 2018.

[36] J. Thilakan, R. Mishra, S. K. Goel, and N. Arya, "Engineering of bone: uncovering strategies of static and dynamic environments," in *Biomaterials in Orthopaedics and Bone Regeneration*, Springer, Singapore, 2019.

[37] H. Qu, H. Fu, Z. Han, and Y. Sun, "Biomaterials for bone tissue engineering scaffolds: a review," *RSC Advances*, vol. 9, no. 45, pp. 26252–26262, 2019.

[38] R. Khalilov, "A comprehensive review of advanced nano-biomaterials in regenerative medicine and drug delivery," *Advances in Biology & Earth Sciences*, vol. 8, no. 1, 2023.

[39] H. Matsuura, M. Sue, M. Takahara, and N. Kuninaga, "Escherichia colirib osteomyelitis," *QJM: An International Journal of Medicine*, vol. 112, no. 1, pp. 35-36, 2019.

[40] K. L. Urish and J. E. Cassat, "Staphylococcus aureus osteomyelitis: bone, bugs, and surgery," *Infection and Immunity*, vol. 88, no. 7, 2020.

[41] C. M. Murphy, M. G. Haugh, and F. J. O'Brien, "The effect of mean pore size on cell attachment, proliferation and migration in collagen–glycosaminoglycan scaffolds for bone tissue engineering," *Biomaterials*, vol. 31, no. 3, pp. 461–466, 2010.